Chapter 8
Mixing States of Ionic Liquid-Molecular Liquid Mixed Solvents and Their Effects on Metal Complex Formation

Toshiyuki Takamuku

Contents

Abstract In this chapter, the complex formation of nickel(II) ion (Ni^{2+}) in imidazolium-based ionic liquids, 1-alkyl-3-methylimidazolium bis(trifluoromethylsulfonyl)amide ($C_N$mimTFSA, *N* represents the alkyl chain length) with molecular liquids (MLs), such as dimethyl sulfoxide (DMSO), methanol (MeOH), and acetonitrile (AN), observed by ultraviolet (UV)-visible spectroscopy is explained on the molecular level. In $C_N$mimTFSA, Ni^{2+} is coordinated with the six oxygen atoms of $TFSA^-$ to form an octahedral complex. On adding ML into the Ni^{2+}-IL solutions, the replacement of the $TFSA^-$ anions by the ML molecules is progressed due to the higher electron donicity of the MLs than that of $TFSA^-$. The stability constants of the complex formation at various temperatures were determined from the UV-visible spectra. It is expected that the mixing state of IL and ML, including the various microscopic interactions, such as IL-cation-anion, IL-cation-ML, and IL-anion-ML, and ML-ML, may influence the complex formation equilibria. Moreover, the polar domains consisting of the charged imidazolium ring and $TFSA^-$ and the nonpolar domains arising from the non-charged alkyl chains may also affect the equilibria. To discuss the mechanism of the complex formation equilibria, thermodynamic

T. Takamuku (✉)
Faculty of Science and Engineering, Saga University, Saga, Japan
e-mail: takamut@cc.saga-u.ac.jp

K. Nishiyama et al. (eds.), *Molecular Basics of Liquids and Liquid-Based Materials*, Physical Chemistry in Action,
https://doi.org/10.1007/978-981-16-5395-7_8

parameters, enthalpies $\Delta H°$ and entropies $\Delta S°$, were estimated using the van't Hoff plots on the stability constants of the complex formation. Moreover, the microscopic interactions were also clarified using infrared (IR), ^{1}H and ^{13}C NMR, small-angle neutron scattering (SANS) techniques.

Keywords Metal complex formation · Imidazolium ring · Electron donicity · Stability constant · Enthalpy · Entropy · Ionic liquid · Dimethyl sulfoxide (DMSO) · Methanol · Acetonitrile · Nickel(II) ion · Complex formation · Solvation · Hydrogen bond · Cluster · UV-visible spectroscopy · NMR · X-ray crystallography · Small-angle neutron scattering (SANS) · Correlation length · van't Hoff plot

8.1 Introduction

Despite electrolytes consisting of organic cation and large-sized anion, room temperature ionic liquids (ILs) are in a liquid state below 100 °C and have unique properties. Particularly, many researchers have paid their attention to the very low volatility and nonflammability of ILs. Thus, ILs may be applied to metal ions extraction, such as noble metals, gold, platinum, and palladium, as a green extractant. Among various kinds of ILs, imidazolium-based ILs have been most often investigated in the fields of chemistry. Figure 8.1 shows the structure of typical imidazolium-based IL, 1-alkyl-3-methylimidazolium bis(trifluoromethylsulfonyl)amide. Here, the IL is abbreviated into $C_N$mimTFSA. $C_N$mimTFSA can be easily synthesized with various alkyl chain lengths N. The previous MD studies showed that the charged imidazolium ring and anion, which is not limited to $TFSA^-$, form the polar domains in pure ILs, whereas the alkyl chains aggregate with themselves to form the nonpolar domains, that is, microphase separation of both domains occurs in neat ILs [1, 2]. In $C_N$mimTFSA, the transition metal ion, such as Ni^{2+}, may be coordinated with the six oxygen atoms of $TFSA^-$ to form the octahedral solvate complex [3]. The details of the coordination manner of $TFSA^-$ for the transition metal ions are still controversial [4, 5], i.e., whether $TFSA^-$ anions coordinate with a transition metal ion as monodentate or bidentate ligands or their mixture in ILs. The crystal structure of cobalt(II) (Co^{2+}) complex, $(C_1C_4Pyr)_2[Co(tfsa)_4]$, precipitated from ionic liquid, 1-butyl-1-methyl-pyrrolidinium $TFSA^-$ (C_1C_4PyrTFSA), has been reported using X-ray crystallography [6]. In the Co^{2+} complex, two $TFSA^-$ anions coordinate with

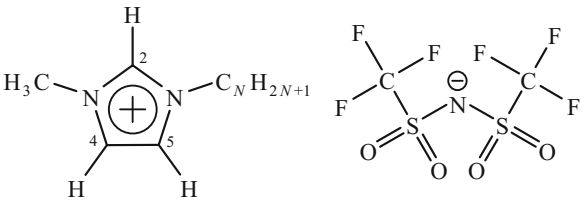

Fig. 8.1 Structure of 1-alkyl-3-methylimidazolium bis(trifluoromethylsulfonyl) amide, $C_N$mimTFSA, where N is the length of the alkyl group

Co^{2+} at the axial positions as monodentate ligands, while the other two anions are bound to the metal ion at the equatorial positions as bidentate ligands to form two chelated rings. Recently, the structure of Co^{2+} solvate complex in the C_4mimTFSA solution was determined by means of extended X-ray fine structure (EXAFS) [7]. In the C_4mimTFSA solution, the six oxygen atoms of six $TFSA^-$ anions coordinate with Co^{2+} as monodentate ligands. However, the coordination of six $TFSA^-$ anions as monodentate ligands is evidenced only from the number of six interactions between the central Co^{2+} and the nonbonding $TFSA^-$ nitrogen atoms.

Various molecular liquids (MLs), such as water and protic and aprotic organic solvents, often have higher basicity (electron donicity) than ILs-anions. For example, the Gutmann's electron-donor numbers D_N [8], which are a scale of basicity, of dimethyl sulfoxide (DMSO), methanol (MeOH), and acetonitrile (AN) (29.8, 19.0, and 14.1, respectively) are much higher than that (7.0) of $TFSA^-$ [9, 10]. Therefore, on adding ML into a metal ion-$C_N$mimTFSA solution, the complex formation equilibrium occurs as a ligand exchange reaction.

Several interactions among metal ion, IL-cation and anion, and ML influence such complex formation equilibrium. In the case of $C_N$mimTFSA, the sizes of polar and nonpolar domains in the solution due to the intrinsic microphase separation of ILs may also affect the equilibrium. Additionally, the three imidazolium ring hydrogen atoms may be hydrogen-bonded with the electron-donor atom of MLs, such as the oxygen atom of DMSO and MeOH and the nitrogen atom of AN [11–13]. On the contrary, protic MLs molecules like MeOH may be hydrogen-bonded with $TFSA^-$ oxygen atoms. Aggregation of ML molecules with themselves may also act on the complex formation, that is, MeOH molecules are hydrogen-bonded with themselves to form MeOH clusters in ILs [14].

However, there have been a few reports on complex formation equilibria for transition metal ions in ILs. The stability constants of the complex formation of uranyl cation $UO_2{}^{2+}$ with nitrate ions $NO_3{}^-$ in C_4mimTFSA have been determined using UV-visible spectroscopy [15]. The structure of the uranyl complex has been observed by an EXAFS technique. The highest complex, $[UO_2(NO_3)_3]^-$, where $NO_3{}^-$ ions coordinate to the uranyl cation as bidentate ligands, formed in the IL solutions [15]. The thermodynamic parameters, enthalpies $\Delta H°$ and entropies $\Delta S°$, of the complex formation of Ni^{2+} with $NO_3{}^-$ anions have been determined from microcalorimetric measurements [16]. Moreover, Kanzaki et al. have determined the thermodynamic parameters of the complex formation of copper(II) (Cu^{2+}) with chloride Cl^- in C_4mimTfO, where TfO^- is the basic anion of trifluoromethylsulfonate [17]. In C_4mimTfO, Cu^{2+} is coordinated by four TfO^- anions to form the square planar structure. $[CuCl_4]^{2-}$ is formed as the highest complex when the Cl^- concentration rises. Despite such investigations, the mechanism of complex formation of transition metal ions in IL−ML binary solvents has not been discussed in terms of the microscopic interactions among IL-cation and anion and ML molecules on the molecular scale.

In this chapter, our investigations on the complex formation equilibria for Ni^{2+} with MLs including DMSO, MeOH, and AN in C_2mimTFSA and C_8mimTFSA

are introduced as below. The complex formation of Ni^{2+} with MLs was observed from the electron spectra of Ni^{2+} by UV-visible spectroscopy. At various temperatures, the stability constants of the complex formation were determined. The thermodynamic parameters, enthalpies $\Delta H°$ and entropies $\Delta S°$, were estimated by the van't Hoff plots on the stability constants. Furthermore, the hydrogen bonding of the imidazolium ring with ML molecules was evaluated using infrared (IR) spectroscopy and ^{1}H and ^{13}C NMR. The aggregation of ML molecules in the ILs was mesoscopically observed by means of small-angle neutron scattering (SANS). The mechanism of the complex formation of Ni^{2+} with ML molecules is discussed in terms of both thermodynamic parameters and interactions among ILs and MLs.

8.2 X-Ray Crystallography

The following X-ray crystallographic data are evidence of the ligand replacement of $TFSA^-$ on Ni^{2+} by ML molecules in the imidazolium-based IL. Figure 8.2 illustrates the structure of $[Ni(dmso)_6](TFSA)_2$ and $[Ni(an)_6](TFSA)_2$, which were precipitated from C_2mimTFSA-DMSO and C_2mimTFSA-AN solutions of $Ni(TFSA)_2$, respectively [18]. For comparison, the structure of $[Co(dmso)_6](TFSA)_2$ is also depicted in the figure. Ni^{2+} and Co^{2+} are coordinated by six DMSO or AN molecules to form an octahedral complex. However, $TFSA^-$ is not bound to the central metal ion. This is because the electron donicities of DMSO and AN are higher than that of $TFSA^-$ as described above. In the structure of both DMSO complexes, the orientation of DMSO molecules suggests that they coordinate with the metal ions through the lone pair of oxygen atoms. AN molecules bind to the metal ion by the lone pair of nitrogen atoms. The octahedral complexes, $[Ni(dmso)_6](TFSA)_2$, $[Ni(an)_6](TFSA)_2$, and $[Co(dmso)_6](TFSA)_2$ reveal that $TFSA^-$ anions that initially coordinate with the metal ion in the IL are fully replaced by ML molecules in the IL solutions at the high ML content.

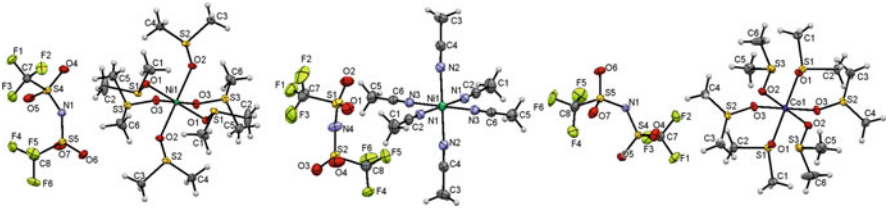

Fig. 8.2 Perspective views of $[Ni(dmso)_6](TFSA)_2$ (left), $[Ni(an)_6](TFSA)_2$ (middle), and $[Co(dmso)_6](TFSA)_2$ (right) complexes, respectively [18]. Thermal ellipsoids are drawn at the 50% probability level. The Cambridge Crystallographic Data Center (CCDC), 1427034, 1427034, and 1427036 contain the supplementary crystallographic data for the complexes, respectively

8.3 Stability Constants

UV-visible spectra for $Ni(TFSA)_2$-$C_N$mimTFSA-ML solutions with $N = 2$ and 8 in the temperature range of 25.0–45.0 °C were recorded as a function of ML content. The MLs include DMSO, MeOH, and AN. Figure 8.3 shows the representative spectra of $Ni(TFSA)_2$ in C_8mimTFSA-ML solutions at the concentration of $[Ni^{2+}] = 50$ mM ($\equiv$ mmol dm^{-3}) and 25.0 °C as a function of ML content [19]. The spectra suggest that the octahedral structure of Ni^{2+} is kept in all the ML systems in the ML concentration range examined. The *d*-*d* transition band in the wavelength range from 600 to 900 nm gradually shifts to the shorter wavelength as the ML content increases. The shifts of both bands at 420 and ~800 nm for the AN solutions with increasing ML concentration are most significant among the three ML systems. This is because the coordination atoms change from the $TFSA^-$ oxygen atoms to the AN nitrogen atoms. These features were also observed for the $Ni(TFSA)_2$-C_2mimTFSA-ML solutions. The UV-visible spectra indicate that $TFSA^-$ anions that initially coordinate with Ni^{2+} are gradually replaced by ML molecules with increasing ML content with keeping the octahedral structure of Ni^{2+}. As shown in Fig. 8.2 of the previous section, six ML molecules may finally coordinate with Ni^{2+} as the highest complex. Thus, the equilibrium can be described as

$$\left[\mathrm{Ni(tfsa)}_m\right] + 6\mathrm{ML} \rightleftharpoons \left[\mathrm{Ni(ml)}_6\right]^{2+} + m\mathrm{TFSA}, \tag{8.1}$$

and the overall stability constant β_6 can be defined by

$$\beta_6 = \frac{\left[\mathrm{Ni(ml)}_6\right]}{[\mathrm{Ni}]\,[\mathrm{ML}]^6}, \tag{8.2}$$

where the IL-anion $TFSA^-$ as a solvent and the charges of species are omitted.

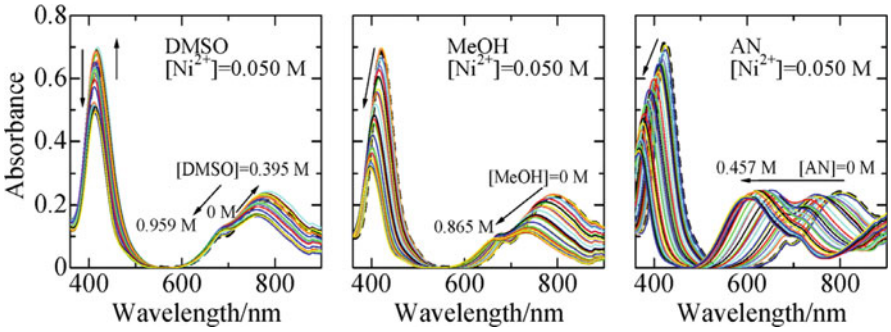

Fig. 8.3 UV-visible spectra of $Ni(TFSA)_2$-C_8mimTFSA solutions with DMSO, MeOH, and AN at 25.0 °C and various ML concentrations [19]. The arrows give the increase in the ML concentration. M represents the units of mol dm^{-3}

The conditional β_n values for the solutions can be determined by fits of the experimental UV-visible spectra at various ML concentrations with Eqs. (8.3), (8.4), and (8.5) for the theoretical absorption of the solutions and the mass balances of Ni^{2+} and ML, respectively.

$$A_{\mathrm{calc},\lambda,n} = \varepsilon_{\mathrm{Ni}^{2+},\lambda}\left[\mathrm{Ni}^{2+}\right] + \varepsilon_{\mathrm{ML},\lambda}\ [\mathrm{ML}] + \sum_{i}^{n} \varepsilon_{n,\lambda}\ \beta_n \left[\mathrm{Ni}^{2+}\right][\mathrm{ML}]^n, \tag{8.3}$$

$$C_{\mathrm{Ni}^{2+}} = \left[\mathrm{Ni}^{2+}\right] + \sum_{n} \beta_n \left[\mathrm{Ni}^{2+}\right][\mathrm{ML}]^n, \tag{8.4}$$

$$C_{\mathrm{ML}} = [\mathrm{ML}] + \sum_{n} n\beta_n \left[\mathrm{Ni}^{2+}\right][\mathrm{ML}]^n, \tag{8.5}$$

where ε represents the molar absorption coefficient for each species as a function of wavelength λ. The spectra in the wavelength range of $\lambda = 360$–900 nm were fitted using the program for nonlinear least-squares refinement with Marquardt algorithm [20], MQSPEC [21] arranged for batch measurements, to minimize the residual U of Eq. (8.6),

$$U = \sum_{\lambda} \sum_{n} \left(A_{\mathrm{exp},\lambda,n} - A_{\mathrm{calc},\lambda,n}\right)^2. \tag{8.6}$$

The ε and β_n values can be refined in the fits. From the UV-visible spectra at several temperatures in the range from 25.0 to 45.0 °C, the β_n values at each temperature were determined. The stepwise stability constants K_n for the equilibria were calculated from the β_n values. The van't Hoff plots were conducted on the $\ln K_n$ values against the reciprocal absolute temperatures to estimate the conditional enthalpies ΔH°_n and entropies of the complex formations in the solutions.

Table 8.1 shows the overall and stepwise stability constants, $\log\beta_n$, and $\log K_n$, respectively, the ΔH°_n and $T\Delta S^\circ_n$ values for the Ni^{2+} complex formation with DMSO, MeOH, and AN in both C_2mimTFSA and C_8mimTFSA at 25.0 °C. The fits of the UV-visible spectra of the MeOH and AN systems with both ILs gave the results of the formation of the di-, tetra-, and hexa-ML complexes, $[Ni(ml)_2]$, $[Ni(ml)_4]$, and $[Ni(ml)_6]$, where the charges of complexes and the coordinated $TFSA^-$ are omitted. For the DMSO system, the formation of the mono-DMSO complex, [Ni(dmso)], is found only in C_8mimTFSA with the longer octyl group.

Table 8.1 Thermodynamic quantities, $\log(\beta_n\ \mathrm{mol}^{-n}\ \mathrm{dm}^{3n})$, $\log(K_n\ \mathrm{mol}^{-2}\ \mathrm{dm}^{6})$, $\Delta H^\circ{}_n$/kJ mol^{-1} and $T\Delta S^\circ{}_n$/kJ mol^{-1} of $[\mathrm{Ni(dmso)}_n]$, $[\mathrm{Ni(meoh)}_n]$, and $[\mathrm{Ni(an)}_n]$ in C_2mimTFSA and C_8mimTFSA solutions at 25.0 °C. The values in the parentheses are standard deviations

	C_2mimTFSA[a]			C_8mimTFSA[b]		
	$[\mathrm{Ni(dmso)}_n]$ $[\mathrm{Ni}^{2+}] = 66$ mM	$[\mathrm{Ni(meoh)}_n]$ $[\mathrm{Ni}^{2+}] = 100$ mM	$[\mathrm{Ni(an)}_n]$ $[\mathrm{Ni}^{2+}] = 100$ mM	$[\mathrm{Ni(dmso)}_n]$ $[\mathrm{Ni}^{2+}] = 50$ mM	$[\mathrm{Ni(meoh)}_n]$ $[\mathrm{Ni}^{2+}] = 50$ mM	$[\mathrm{Ni(an)}_n]$ $[\mathrm{Ni}^{2+}] = 50$ mM
$\log\beta_1$				5.18(18)		
$\log\beta_2$	9.48(88)	3.89(3)	5.72(2)	10.11(35)	5.00(7)	7.69(16)
$\log\beta_4$	19.03(1.76)	8.25(5)	10.62(4)	16.03(37)	10.30(15)	14.91(32)
$\log\beta_6$	27.26(2.64)	11.73(7)	14.40(5)	19.42(39)	15.23(21)	20.82(48)
$\log K_1$				5.18(18)		
$\log K_2$	9.48(88)	3.89(3)	5.72(2)	4.93(17)	5.00(7)	7.69(16)
$\log K_4$	9.55(88)	4.37(4)	4.90(2)	5.92(3)	5.29(7)	7.21(16)
$\log K_6$	8.23(88)	3.47(2)	3.78(2)	3.39(1)	4.93(6)	5.91(16)
$\Delta H^\circ{}_1$				−122(13)		
$\Delta H^\circ{}_2$	−130(14)	−60(4)	−58.8(9)	−153(14)	−73(6)	−115(19)
$\Delta H^\circ{}_4$	−126(11)	−52(5)	−60(1)	−72(12)	−81(3)	−111(18)
$\Delta H^\circ{}_6$	−100(13)	−51(2)	−55.6(5)	−39(3)	−58(8)	−91(23)
$T\Delta S^\circ{}_1$				−93(12)		
$T\Delta S^\circ{}_2$	−76(14)	−38(4)	−26.2(9)	−125(13)	−44(6)	−68(18)
$T\Delta S^\circ{}_4$	−71(11)	−27(5)	−32(1)	−39(12)	−51(3)	−71(17)
$T\Delta S^\circ{}_6$	−52(13)	−31(2)	−34.0(4)	−19.5(3.3)	−31(8)	−59(23)

[a]Ref. [18]
[b]Ref. [19]

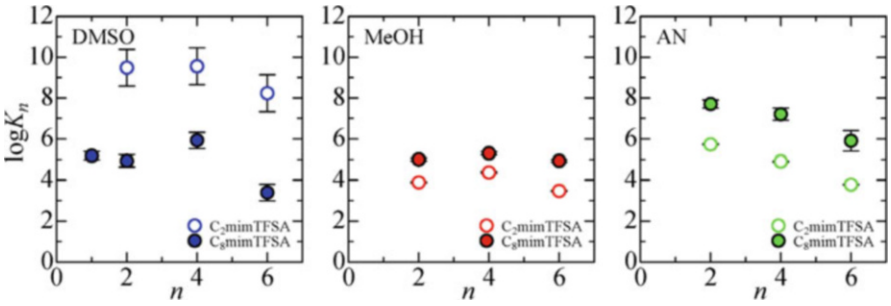

Fig. 8.4 Stepwise stability constants for $[Ni(dmso)_n]$, $[Ni(meoh)_n]$, and $[Ni(an)_n]$ complexes in C_2mimTFSA (open circles) [18] and C_8mimTFSA (filled circles) [19] at 25.0 °C against the equilibrium step n. The standard deviations are represented by error bars

The $\log\beta_6$ values for the highest Ni^{2+} complexes in the C_2mimTFSA solutions with the shorter ethyl chain are larger in the order of $[Ni(dmso)_6]$ > > $[Ni(an)_6]$ > $[Ni(meoh)_6]$. The largest stability of the hexa-DMSO complex $[Ni(dmso)_6]$ is caused by the highest electron donicity of DMSO among the three MLs. The Gutmann's donor numbers of DMSO, MeOH, and AN are D_N = 29.8, 19.0, and 14.1, respectively [8]. Interestingly, the $\log\beta_6$ values in the C_8mimTFSA solutions with the longer octyl chain are larger in the different order of $[Ni(an)_6]$ > $[Ni(dmso)_6]$ > $[Ni(meoh)_6]$ from that of the C_2mimTFSA solutions. Despite the lowest electron donicity, AN molecules form the most stable complex with Ni^{2+} in the C_8mimTFSA solutions. The stability of $[Ni(meoh)_6]$ is the lowest in both IL solutions, although the donor number of MeOH is middle between those of DMSO and AN.

For comparison of the stepwise complex formation in the C_2mimTFSA and C_8mimTFSA solutions, the $\log K_n$ values are plotted against the equilibrium step n in Fig. 8.4. The di-, tetra-, and hexa-AN complexes, $[Ni(an)_2]$, $[Ni(an)_4]$, and $[Ni(an)_6]$, are more stable in the IL with the longer octyl chain compared to those in the IL with the shorter ethyl chain. In contrast, the stabilities of the DMSO complexes, $[Ni(dmso)_2]$, $[Ni(dmso)_4]$, and $[Ni(dmso)_6]$, in the IL with the longer alkyl chain are much lower than those in the IL with the shorter chain. Nevertheless, the mono-DMSO complex, [Ni(dmso)], can only be formed in the IL with the longer chain. Surprisingly, the stabilities of the MeOH complexes in both ILs are not largely different from each other, unless the DMSO and AN complexes. These features on the Ni^{2+} complex formation with ML molecules should be attributed to the microscopic interactions among IL-cation and anion and ML molecules. In the next section, the mixing states of the ILs of C_2mimTFSA and C_8mimTFSA with the three MLs observed by IR, ^{1}H and ^{13}C NMR, SANS techniques are explained on the micro- and mesoscopic scales.

8.4 Mixing States of C_2mimTFSA and C_8mimTFSA with MLs

In the imidazolium-based ILs, the interactions of the positively charged imidazolium ring with ML molecules are important. The three hydrogen atoms of the imidazolium ring may be hydrogen-bonded with MLs. In particular, the hydrogen atom at position 2 between the two nitrogen atoms (see Fig. 8.1) can be most strongly hydrogen-bonded with ML molecules because of its highest positive charge (the highest acidity) among the three hydrogen atoms [22, 23]. The hydrogen bonding of the ring hydrogen atoms with MLs can be evaluated from the redshift of the C-H stretching vibration of the ring and the deshielding of ^{1}H and ^{13}C chemical shifts observed by IR and NMR spectroscopy, respectively. The C-H vibration and the NMR chemical shifts for C_2mimTFSA with DMSO, MeOH, and AN showed that the hydrogen bonds of the ring hydrogen atoms with the MLs are stronger in the order of DMSO > > MeOH > AN [11]. This is consistent with Gutmann's electron-donor number of the MLs [8], as described in the previous section. The mixing state of each ML with $C_N$mimTFSA is discussed in the below sections.

8.4.1 Acetonitrile

The effect of the alkyl chain length of the imidazolium most markedly appears in the AN system due to the lowest electron donicity (the hydrogen bonding acceptability) of the AN nitrogen atom. Figure 8.5 shows the differences of the chemical shifts $\Delta\delta$/ppm of the hydrogen and carbon atoms at the positions of 2, 4, and 5 of the ring in the C_2mimTFSA-AN and C_8mimTFSA-AN solutions from those for neat ILs ($x_{AN} = 0$) as a function of AN mole fraction x_{AN}. At position 2, the $\Delta\delta$ value gradually increases in C_2mimTFSA with the increase in x_{AN}. Thus, the hydrogen atom at the position 2 is deshielded with increasing x_{AN}; that is, the electron density of the hydrogen atom decreases with the increase in AN content. It is suggested that the hydrogen bond between the hydrogen atom and AN strengthens in C_2mimTFSA as the AN content increases. On the contrary, the $\Delta\delta$ value of the hydrogen atom for the C_8mimTFSA-AN solutions decreases with increasing x_{AN}, revealing the shielding of the hydrogen atom. Thus, the hydrogen bond between the hydrogen atom at the position 2 and AN molecule gradually weakens with the increases in the AN content. This difference in the hydrogen bonding of AN molecules between the ILs with the ethyl and octyl groups arises from the steric hindrance of the long alkyl chain.

On the other hand, the $\Delta\delta$ values of the hydrogen and carbon atoms at positions 4 and 5 in both ILs increase with increasing x_{AN}. This is because the cyano group C≡N of AN molecules interacts with the imidazolium ring through the π-π interaction between the ring and the cyano group. The positive charge (the acidity) of the hydrogen atoms at the positions 4 and 5 is lower than that at the

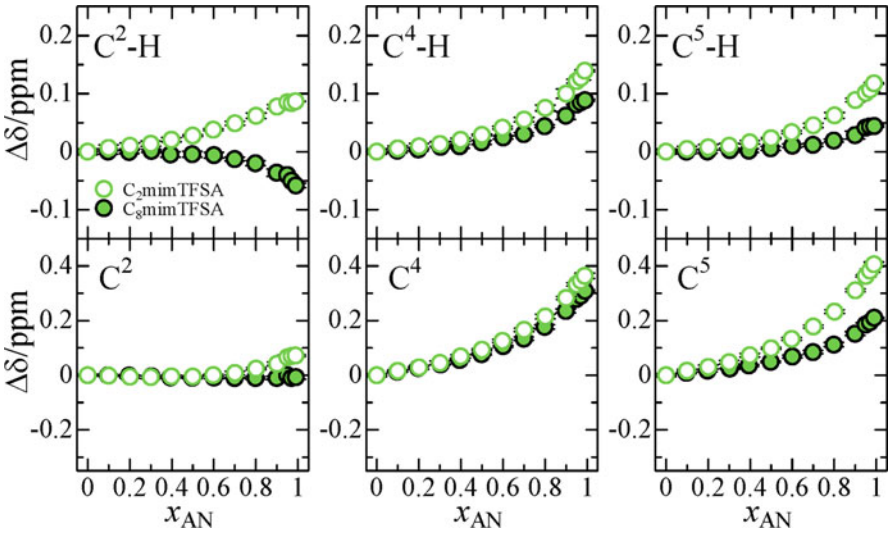

Fig. 8.5 Differences, Δδ/ppm, in ^{1}H and ^{13}C NMR chemical shifts for the C^2-H, C^4-H, and C^5-H positions of the imidazolium ring in C_2mimTFSA-AN and C_8mimTFSA-AN solutions from those at $x_{AN} = 0$ as a function of x_{AN} [19]. The standard deviations are represented by error bars

position 2. Thus, the π-π interaction of the AN cyano group at both positions is predominant rather than hydrogen bonding. When AN molecule interacts with other molecules, the side of the C≡N group gives the magnetical deshielding field, while the lone pair of the AN nitrogen atom provides the shielding field. Thus, the weaker deshielding of the hydrogen and carbon atoms at the positions 4 and 5 in the C_8mimTFSA solutions than in the C_2mimTFSA suggests that the π-π interaction of AN molecules with the ring is weaker in the former than the latter due to the steric hindrance of the longer octyl chain, as well as the hydrogen bond at the position 2. These results reveal that AN molecules in the C_8mimTFSA-AN solutions more weakly interact with the IL than in the C_2mimTFSA-AN solutions. In other words, AN molecules are freer in the former than those in the latter.

8.4.2 MeOH

MeOH molecules can be hydrogen-bonded with the imidazolium ring hydrogen atoms, particularly the atom at the position 2 in the ILs [11]. The left panel of Fig. 8.6 indicates the wavenumber of the C-H stretching vibration at the position 2 in C_2mimTFSA and C_8mimTFSA as a function of MeOH mole fraction x_{MeOH}. Generally, a redshift of the vibration with increasing ML content gives the information on the strengthening of the hydrogen bond of the ring hydrogen atom with ML molecule. As shown in the left panel of Fig. 8.6, however, the redshift

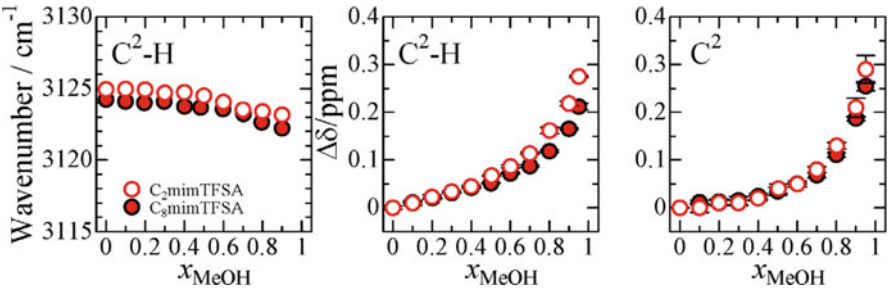

Fig. 8.6 Wavenumbers of the stretching vibrations (left) and differences, Δδ/ppm, in ^{1}H and ^{13}C NMR chemical shifts (middle and right, respectively) for the C^2-H position of the imidazolium ring from those at $x_{MeOH} = 0$ in C_2mimTFSA-MeOH and C_8mimTFSA-MeOH solutions as a function of x_{MeOH} [19]. The standard deviations are represented by error bars

against the increase in x_{MeOH} is not significant in both ILs. The redshift of ~2 cm^{-1} for both MeOH systems with increasing x_{MeOH} from 0 to 0.9 is much less compared to that of ~7 cm^{-1} for C_2mimTFSA-DMSO system in the same mole fraction range in the literature [11]. The hydrogen bond of MeOH with the ring hydrogen atom at the position 2 is weaker than that of DMSO. Furthermore, the difference in the redshifts between the C_2mimTFSA-MeOH and C_8mimTFSA-MeOH solutions is not remarkable. Thus, the strength of the hydrogen bond is not markedly different between the IL solutions. As shown in the middle and right panels of Fig. 8.6, the differential ^{1}H and ^{13}C NMR chemical shifts $\Delta\delta$ of the ring hydrogen and carbon atoms in both IL systems increase with increasing x_{MeOH}. Therefore, the hydrogen bond of the ring hydrogen atom at position 2 with MeOH molecule strengthens as the x_{MeOH} increases. However, the differences in the $\Delta\delta$ values for both IL solutions are very small. This is consistent with the small difference of the C-H stretching vibration at the position. The IR and NMR results reveal that the strength of the hydrogen bond between MeOH and the hydrogen atom at position 2 is not remarkably affected by the alkyl chain length.

In the MeOH case, the self-hydrogen bonds among MeOH molecules should be pointed out rather than the hydrogen bond with the imidazolium ring. In fact, SANS experiments on $C_N$mimTFSA-deuterated MeOH (MeOH-d_4) with $N = 4$–12 showed that the ILs are heterogeneously mixed with MeOH in the high MeOH-d_4 mole fraction range [14]. Figure 8.7 indicates the SANS profiles of $C_N$mimTFSA-MeOH-d_4 solutions at various x_{MeOH}. The correlation lengths ξ of the scale for heterogeneous mixing were estimated from the fits on the SANS profiles through the Ornstein-Zernike equation,

$$I(q) = I_0/(1 + \xi^2 q^2) + \text{b.g.}, \tag{8.7}$$

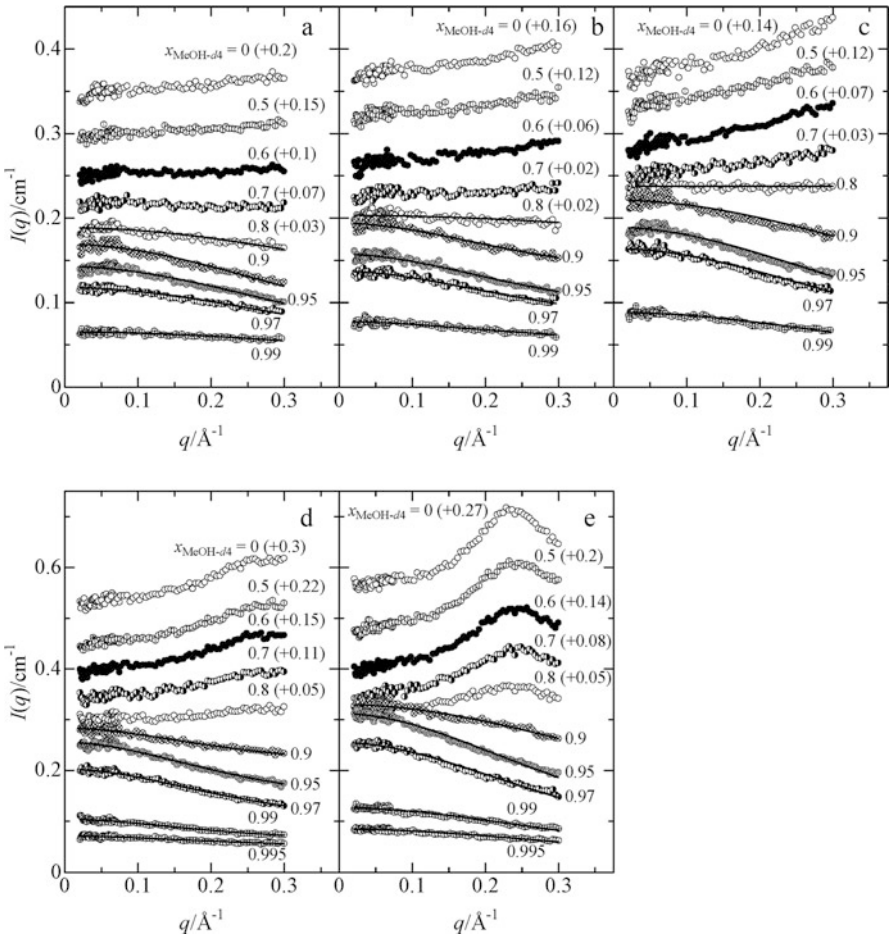

Fig. 8.7 SANS profiles of $C_N$mimTFSA-MeOH-d_4 solutions at various MeOH-d_4 mole fractions ((**a**) $N = 4$; (**b**) 6; (**c**) 8; (**d**) 10; (**e**) 12) [14]. The values in parentheses are those shifted from the origin to avoid overlap of the plots. The solid lines show the results of Ornstein-Zernike fits

where q ($= 4\pi\sin\theta/\lambda$) represents the scattering vector with the scattering angle 2θ and the wavelength of neutrons λ, I_0 gives the scattering intensity at $q = 0$, and b.g. the background intensities. The ξ values are plotted against $x_{MeOH\text{-}d4}$ in Fig. 8.8. As shown in Fig. 8.8, the mole fraction of the maximum heterogeneity for each system appears around $x_{MeOH} = 0.97$. The mole fraction of the maximum ξ does not depend on the alkyl chain length N. However, the magnitude of the maximum heterogeneity for $C_N$mimTFSA-MeOH-d_4 solutions is enhanced with elongating the alkyl chain N. The heterogeneity arises from the self-hydrogen bonding among MeOH to form MeOH clusters in the solutions. Figure 8.9 shows the x_{MeOH} dependence of the concentration ratios of the isolated and hydrogen-

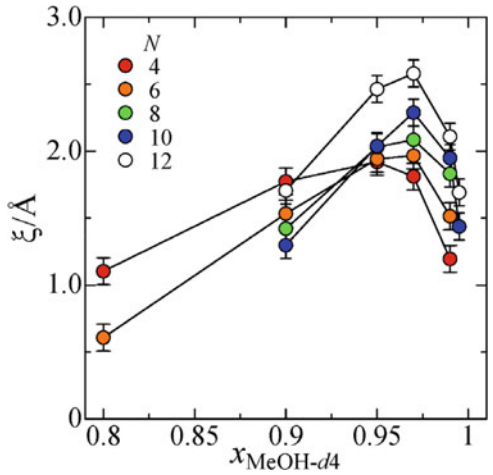

Fig. 8.8 Ornstein-Zernike correlation lengths ξ of $C_N$mimTFSA-MeOH-d_4 solutions as a function of MeOH-d_4 mole fraction [14]. The standard deviations are indicated as error bars

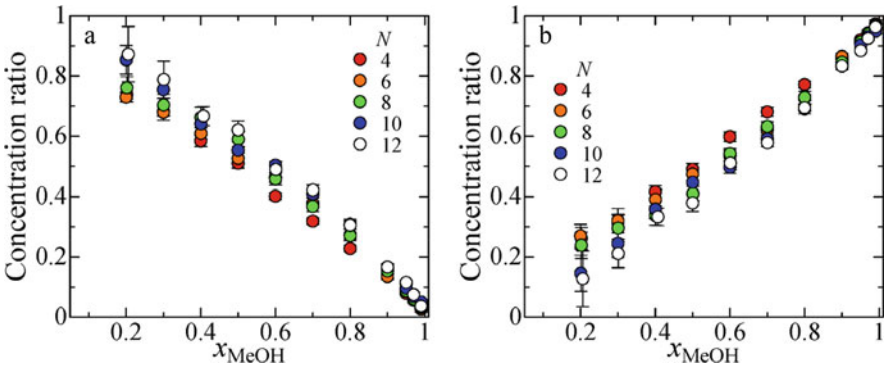

Fig. 8.9 Ratios of the concentrations of (**a**) isolated and (**b**) hydrogen-bonded MeOH molecules to the total concentration of MeOH of $C_N$mimTFSA-MeOH solutions as a function of x_{MeOH} [14]. The standard deviations are indicated as error bars

bonded MeOH molecules, which were estimated from the IR measurements on the O-H stretching vibration modes of MeOH molecules in $C_N$mimTFSA-MeOH solutions [14]. As shown in Fig. 8.9, the concentration of the self-hydrogen-bonded MeOH molecules at each x_{MeOH} decreases with elongating the alkyl chain length N. In contrast, the isolated MeOH molecules increase with the elongation of N. Therefore, MeOH molecules are freer in the C_8mimTFSA-MeOH solutions than in the C_2mimTFSA-MeOH solutions, although the heterogeneity is more enhanced in the C_8mimTFSA solutions. The magnitude of heterogeneity for the IL-MeOH solutions observed by the SANS experiments may mainly arise from the aggregation of the alkyl chains rather than the self-hydrogen bonding of MeOH molecules.

8.4.3 DMSO

DMSO molecules are most strongly hydrogen-bonded with all the three imidazolium ring hydrogen atoms due to the highest electron donicity among the MLs. The strong hydrogen bonds of DMSO with the ring hydrogen atoms bring the homogeneous mixing between $C_N$mimTFSA and DMSO. Figure 8.10 displays the SANS profiles of $C_N$mimTFSA-deuterated DMSO (DMSO-d_6) solutions with the alkyl chain lengths $N = 2$–12 at various DMSO mole fractions $x_{\mathrm{DMSO}\text{-}d6}$ [13].

In the IL-DMSO solutions with $N \geq 6$, a peak is observed in the scattering vector q range from 0.2 to 0.3 $\mathrm{Å}^{-1}$. This is often called as a low-q peak [24]. The peak is more noticeable at the lower $x_{\mathrm{DMSO}\text{-}d6}$ and strengthens with elongating the

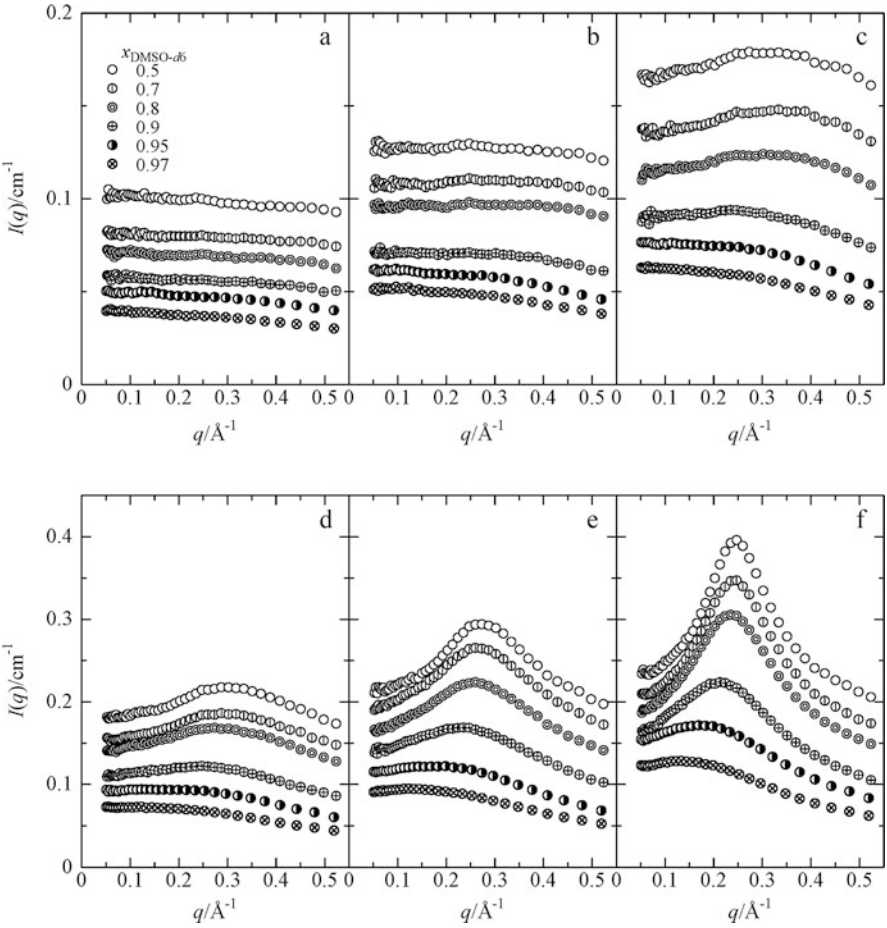

Fig. 8.10 SANS profiles of $C_N$mimTFSA-DMSO-d_6 solutions at various DMSO-d_6 mole fractions ((**a**) $N = 2$; (**b**) 4; (**c**) 6; (**d**) 8; (**e**) 10; (**f**) 12) [13]

alkyl chain length N. Moreover, the peak shifts to the lower q as the alkyl chain N lengthens. These findings agree with the X-ray diffraction results on $C_N$mimCl and $C_N$mimBF_4 with $N = 4$–10 [25] and the SANS results on $C_N$mimTFSA with $N = 6$–12 [24]. In the imidazolium-based ILs, the polar domains consisting of the charged imidazolium rings and anions and the nonpolar domains of aggregation of the alkyl chains are simultaneously formed, as described above [1, 2]. The SANS and high-energy X-ray diffraction (HEXRD) study with the help of MD simulations suggested that the low-q peak mainly arises from the diffraction caused by the inter-aggregates of the polar domains, but not the nonpolar domains consisting of the alkyl chains [24].

Nevertheless, the significant SANS intensities of the Ornstein-Zernike type are not observed in the profiles of $C_N$mimTFSA-DMSO-d_6 solutions below $q = 0.2$ Å^{-1} (Fig. 8.10), unlike the MeOH system (Fig. 8.7). Thus, DMSO molecules are homogeneously mixed with the ILs, at least on the SANS scale. This is due to the strong hydrogen bonds of DMSO with the ring hydrogen atoms. It is likely, therefore, that DMSO molecules more frequently exist in the polar domains of ILs formed by the charged imidazolium rings and anions than the nonpolar domains of the alkyl chains.

8.5 Mechanism of Complex Formation

In this section, the complex formation equilibria of Ni^{2+} with the three MLs, DMSO, MeOH, and AN in C_2mimTFSA and C_8mimTFSA are discussed, according to the thermodynamic parameters and the mixing states of the IL-ML solutions explained above. In particular, the effects of the alkyl chain length N of the ILs on the complex formation are discussed on the molecular scale.

Figure 8.11 indicates the stepwise ΔH°_n and $T\Delta S^\circ_n$ values for the DMSO, MeOH, and AN systems with both C_2mimTFSA and C_8mimTFSA at 25.0 °C against the equilibrium step n, which are listed in Table 8.1. As shown in Table 8.1 and Fig. 8.4, the $\log K_n$ values of the AN systems reveal that the di-, tetra-, and hexa-AN complexes are more stable in C_8mimTFSA with the longer octyl chain than in C_2mimTFSA with the shorter ethyl chain. As discussed in the Sect. 8.4.1, AN molecules in the former IL are freer than those in the latter IL. AN molecules do not strongly hydrogen-bonded with the imidazolium ring because of the low electron donicity. Particularly, the hydrogen bonding of AN with the ring hydrogen atoms in the IL with the octyl chain is weaker compared to that in the IL with the ethyl chain due mainly to the steric hindrance of the longer octyl chain. Moreover, the octyl chain weakens the π-π interaction between the AN cyano group and the ring at the positions 4 and 5. The disruption for the weaker interactions of the imidazolium ring with AN molecules in the C_8mimTFSA solutions does not cause the large enthalpic loss, when AN molecules are bound to Ni^{2+}. In contrast, the stronger interaction of AN with the imidazolium ring in the C_2mimTFSA solutions results in the larger enthalpic loss for the coordination of AN with Ni^{2+}. Thus, as shown in Fig. 8.11,

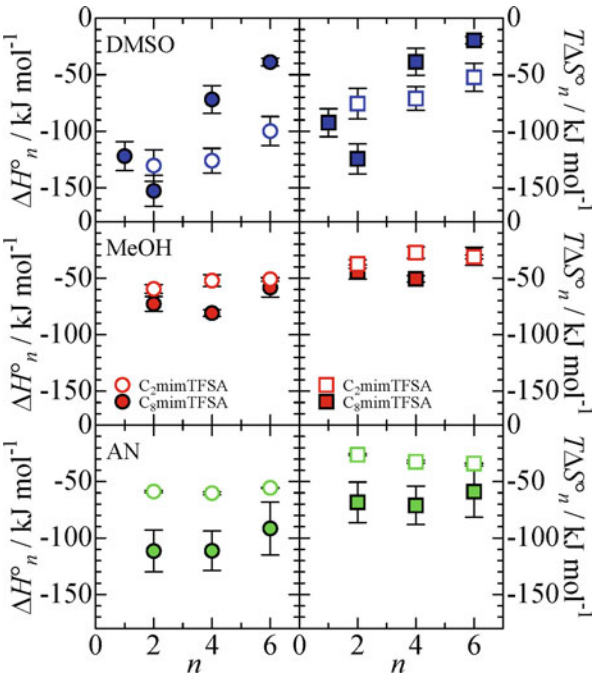

Fig. 8.11 Stepwise ΔH°_n (left) and $T\Delta S^\circ_n$ at 25.0 °C (right) for $[Ni(dmso)_n]$, $[Ni(meoh)_n]$, and $[Ni(an)_n]$ complexes in C_2mimTFSA (open symbols) [18] and C_8mimTFSA (filled symbols) [19]. The standard deviations are represented as error bars

the ΔH°_n values for all the three steps for the C_8mimTFSA-AN solutions are more negative than those in the C_2mimTFSA-AN solutions. From the entropic aspects, the loss of the degree of freedom for AN molecules in the C_8mimTFSA solutions is larger than that of the C_2mimTFSA solutions because of the restriction of freer AN molecules on Ni^{2+}. Indeed, the $T\Delta S^\circ_n$ values for the former solutions are more negative compared to those for the latter solutions. For both IL solutions, the magnitude of ΔH°_n values is larger than those of $T\Delta S^\circ_n$ values. Thus, the complex formation of $[Ni(an)_n]$ is enthalpically driven in both ILs. The more negative ΔH°_n values for the C_8mimTFSA solutions than the C_2mimTFSA solutions contribute to the higher stability of the complexes in the AN systems.

Figure 8.4 shows that the $\log K_n$ values for the MeOH systems with both ILs do not significantly differ from each other. The strength of the hydrogen bonding of MeOH with the imidazolium ring hydrogen atoms, especially at the position 2, is not markedly different between the two IL solutions. As shown in the SANS results, MeOH molecules are self-hydrogen-bonded with themselves to form MeOH clusters in the ILs. Thus, the self-hydrogen bonding among MeOH molecules is the key to the thermodynamics of the equilibria. As described in the Sect. 8.4.2, MeOH clusters are more enhanced in the IL with the longer alkyl chain *N*. However, this mainly arises from the aggregation of the alkyl chain rather than the self-hydrogen bonding among MeOH. In fact, the IR spectroscopic experiments suggested that the self-hydrogen bonds among MeOH molecules decrease with elongating the alkyl chain of IL. Thus, the self-hydrogen bonds in the C_8mimTFSA-MeOH solutions

are weaker than in the C_2mimTFSA-MeOH solutions. This is reflected in the thermodynamic parameters as described below.

As seen in Fig. 8.11, the ΔH°_n values at the steps of $n = 2$ and 4 in the C_8mimTFSA solutions are slightly more negative than those in the C_2mimTFSA solutions. The $T\Delta S^\circ_n$ value at the step of $n = 4$ in the former is lower than that in the latter. Additionally, the value at $n = 2$ for the former is also slightly lower than that for the latter. These thermodynamic features arise from the higher degree of freedom of MeOH molecules in the C_8mimTFSA-MeOH solutions due to the weaker self-hydrogen bonds among MeOH molecules. The coordination of MeOH with Ni^{2+} in the C_8mimTFSA solutions is more significantly reflected in the enthalpic gain than in the C_2mimTFSA solutions. This oppositely results in the effect on the entropic loss. However, the strength of the self-hydrogen bonds among MeOH is not sufficiently different between both IL solutions to cause a large difference in the stability constants of the Ni^{2+} complexes in the solutions. The difference between the enthalpic gain and the entropic loss in both IL-MeOH solutions is comparable with each other. Thus, the $\log K_n$ values at $n = 2$ and 4 for the two IL-MeOH systems are coincident with each other. Figure 8.11 also shows that the enthalpic gain in the C_8mimTFSA-MeOH solutions at $n = 6$ becomes smaller than those at $n = 2$ and 4. The entropic loss at $n = 6$ is smaller than those at $n = 2$ and 4. The changes in the ΔH°_n and $T\Delta S^\circ_n$ values from $n = 4$ to 6 are caused by the strengthened self-hydrogen bonds among MeOH molecules due to the increase in the MeOH content in the C_8mimTFSA-MeOH solutions where the hexa-MeOH complex mainly forms.

For the DMSO systems, as shown in Fig. 8.4, the $\log K_n$ values for the C_8mimTFSA-DMSO solutions are remarkably smaller than those for the C_2mimTFSA-DMSO solutions, while, for the MeOH and AN systems, the former values are larger than the latter values though the difference between the former and latter values for the MeOH systems is very small. Furthermore, the mono-DMSO complex forms in the C_8mimTFSA-DMSO solutions. DMSO molecules can be strongly hydrogen-bonded with the three imidazolium ring hydrogen atoms. The strong hydrogen bonds may not be affected by the alkyl chain length N of the ILs [13]. Thus, the other factors may contribute to the difference of the stability constants of Ni^{2+} complex formation with DMSO in the ILs. As described in the Sect. 8.4.3, the polar domains consisting of the imidazolium rings and anions are formed by the electrostatic force in the imidazolium-based ILs, while the nonpolar domains of aggregates of the alkyl groups are generated through the dispersion force [1, 2]. As the alkyl group elongates, the volume of the nonpolar domains in the ILs increases. However, the volume of the polar domains does not change with the alkyl chain length. Thus, the volume ratio of the polar domains to the nonpolar domains in the ILs decreases against the elongation of the alkyl chain N.

Ni^{2+} and DMSO may be concentrated into the polar domains in the ILs because of the charge and the strong hydrogen bonding with the ring hydrogen atoms, respectively. The ligand exchange reaction of $TFSA^-$ on Ni^{2+} by DMSO molecules mainly occurs in the polar domains of the IL-DMSO solutions. As the alkyl chain of $C_N$mimTFSA elongates from the ethyl to the octyl group, the ligand exchange reaction should take place in the smaller spaces of the polar domains. This is the

same even in the MeOH and AN systems. However, DMSO molecules are the most strongly hydrogen-bonded with the imidazolium ring hydrogen atoms. Therefore, the largest DMSO molecules may be most significantly affected by the smaller spaces of the polar domains among the three MLs. DMSO molecules are less easily eliminate from the ring in the smaller polar domains of C_8mimTFSA than C_2mimTFSA. $TFSA^-$ may not also easily dissociate from Ni^{2+} due to the smaller spaces of the polar domains. These factors contribute to the formation of the mono-DMSO complex in the C_8mimTFSA solutions. In the mono-DMSO complex, at least one $TFSA^-$ anion may coordinate with Ni^{2+} as a monodentate ligand with an opened chelate ring. The confined spaces also contribute to the smaller $\log K_n$ of the higher complexes at $n = 4$ and 6 in the C_8mimTFSA solutions. Therefore, the ΔH°_n values in the C_8mimTFSA solutions at $n = 4$ and 6 are less negative as compared to those in the C_2mimTFSA solutions due to the larger enthalpic loss for the disruption of the bonds between Ni^{2+} and the $TFSA^-$ oxygen atoms in the C_8mimTFSA solutions. The less negative $T\Delta S^\circ_n$ values at $n = 4$ and 6 may be ascribed to the increase in the degree of freedom for $TFSA^-$ eliminated from Ni^{2+}. Consequently, the stabilities of the di-, tetra-, and hexa-DMSO complexes in the C_8mimTFSA solutions are lower than those in the C_2mimTFSA solutions.

8.6 Conclusions

The present investigations showed that the complex formation of Ni^{2+} with MLs of DMSO, MeOH, and AN occurs in the imidazolium-based ILs of C_2mimTFSA and C_8mimTFSA. The $TFSA^-$ anions of the ILs that initially solvate to Ni^{2+} are replaced by ML molecules in the three steps with increasing ML content. When the ML concentration increases, a pair of ML molecules simultaneously replace $TFSA^-$ at each step. Therefore, the di- and tetra-ML complexes, $[Ni(ml)_2]$ and $[Ni(ml)_4]$ were formed in the ILs. Then, the hexa-ML complex, $[Ni(ml)_6]$, was finally formed in the ILs at the high ML content. Based on the present results only, it appears that three $TFSA^-$ anions are bound to Ni^{2+} via the two oxygen atoms as bidentate ligands to form the solvated complex $[Ni(tfsa)_3]^{2+}$ with the three chelate rings in the ILs. Interestingly, the mono-DMSO complex, [Ni(dmso)], is only formed in C_8mimTFSA with the longer octyl chain. In the complex formation, the microscopic interactions affect each step depending on the properties of ILs and MLs.

In C_2mimTFSA with the shorter ethyl chain, the stability of the complexes with MLs is higher in the order of DMSO >> AN > MeOH. The highest stability of the DMSO complexes mainly arises from the highest electron donicity of DMSO among the MLs. However, despite the higher electron donicity of MeOH than that of AN, the MeOH complexes are less stable compared to the AN complexes. The self-hydrogen bonding among MeOH molecules to form MeOH clusters affects on the lower stability of the MeOH complexes. These features of the ML complex formation in C_2mimTFSA are not surprising. In other words, the mechanism of the ML complex formation in the IL can be understood in terms of the interactions

of IL-ML and ML-ML, as well as the mechanism of the complex formation in conventional solvents.

The specific properties of the imidazolium-based ILs appeared in the complex formation of Ni^{2+} with the MLs in C_8mimTFSA with the longer octyl chain rather than C_2mimTFSA. The stability of the DMSO complexes became lower than that of the AN complex. Furthermore, the formation of the mono-DMSO complex was found in C_8mimTFSA. These findings for the DMSO system are attributed to the microphase separation of the imidazolium-based ILs. In the ILs, the positively charged imidazolium rings and anions form the polar domain, whereas the alkyl chains aggregate with themselves to form the nonpolar domain. The volume ratio of the polar domains against the nonpolar ones in the ILs decreases with elongating the alkyl chain because of the development of the nonpolar domains. Thus, the spaces of the polar domains in C_8mimTFSA are smaller than those in C_2mimTFSA. The complex formation takes place in the polar domains, where Ni^{2+}, $TFSA^-$, and DMSO are condensed. In the smaller spaces of C_8mimTFSA, the replacement of $TFSA^-$ coordinated with Ni^{2+} by DMSO less easily occurs than in C_2mimTFSA. This is the plausible reason for the lower stability of the DMSO complexes and the formation of the mono-DMSO complex in C_8mimTFSA. In the AN systems, the degree of freedom of AN is increased in C_8mimTFSA because of the weaker interaction between AN molecules and the imidazolium ring. Thus, the enthalpic gain of the coordination of AN with Ni^{2+} largely contributes to the higher stability of the AN complexes in C_8mimTFSA than C_2mimTFSA.

In both C_2mimTFSA and C_8mimTFSA, the MeOH clusters due to the self-hydrogen bonding among MeOH molecules mainly affected the lowest stability of the MeOH complexes among the three ML systems. The self-hydrogen bonds among MeOH molecules become weaker in C_8mimTFSA than C_2mimTFSA. However, the enthalpic loss for the disruption of the self-hydrogen bonds among MeOH molecules is not significantly different between the two IL systems. Thus, the effect of the alkyl chain length of the IL-cations on the complex formation did not markedly appear, resulting in the smallest difference in the stability of the MeOH complexes among the ML complexes.

As discussed above, the properties of the imidazolium-based ILs observed by IR, NMR, and SANS were reflected in the complex formation of Ni^{2+} with the three MLs. For the application of ILs as extractants, further investigations on the complex formation of the transition metal ions in ILs on the molecular scale should be needed. The present investigations are the first case of such studies connecting the complex formation with the properties of IL-ML binary solvents.

Acknowledgments This work was supported partly by JSPS KAKENHI (Grant Nos. 199550022, 22550018, 26410018 and 18K05038). The density and NMR measurements were conducted at the Analytical Research Center for Experimental Sciences of Saga University supported by "Project for Promoting Public Utilization of Advanced Research Infrastructure." The SANS experiments on the MeOH system were carried out in joint research with the Institute for Solid State Physics, the University of Tokyo (Proposal No. 8851). The SANS experiments on the DMSO system were performed with the approval of the Neutron Program Review Committee of J-PARC/MLF (Proposal No. 2017A0002).

References

1. Lopes JNC, Padua AA (2006) Nanostructural organization in ionic liquids. J Phys Chem B 110:3330–3335
2. Jiang W, Wang Y, Voth GA (2007) Molecular dynamics simulation of nanostructural organization in ionic liquid/water mixtures. J Phys Chem B 111:4812–4818
3. Fujii K, Nonaka T, Akimoto Y, Umebayashi Y, Ishiguro S (2008) Solvation structures of some transition metal(II) ions in a room-temperature ionic liquid, 1-ethyl-3-methylimidazolium bis(trifluoromethanesulfonyl)amide. Anal Sci 24:1377–1380
4. Bortolini O, Chiappe C, Ghilardi T, Massi A, Pomelli CS (2014) Dissolution of metal salts in bis(trifluoromethylsulfonyl)imide-based ionic liquids: studying the affinity of metal cations toward a "weakly coordinating" anion. J Phys Chem A 119:5078–5087
5. Liu T, Danten Y, Grondin J, Vilar R (2016) Solvation of AgTFSI in 1-ethyl-3-methylimidazolium bis(trifluoromethylsulfonyl)imide ionic liquid investigated by vibrational spectroscopy and DFT calculations. J Raman Spectrosc 47:449–456
6. Nockemann P, Pellens M, Van Hecke K, Van Meervelt L, Wouters J, Thijs B, Vanecht E, Parac-Vogt TN, Mehdi H, Schaltin S, Fransaer J, Zahn S, Kirchner B, Binnemans K (2010) Cobalt(II) complexes of nitrile-functionalized ionic liquids. Chem Eur J 16:1849–1858
7. Busato M, D'Angelo P, Lapi A, Tolazzi M, Melchior A (2020) Solvation of Co^{2+} ion in 1-butyl-3-methylimidazolium bis(trifluoromethylsulfonyl)imide ionic liquid: a molecular dynamics and X-ray absorption study. J Mol Liq 299:112120
8. Gutmann V (1978) The donor-acceptor approach to molecular interactions. Plenum Press, New York
9. Yamagata M, Katayama Y, Miura T (2006) Electrochemical behavior of samarium, europium, and ytterbium in hydrophobic room-temperature molten salt systems. J Electrochem Soc 153:E5–E9
10. Zhu Y-L, Katayama Y, Miura T (2010) Effects of acetonitrile on electrodeposition of Ni from a hydrophobic ionic liquid. Electrochim Acta 55:9019–9023
11. Takamuku T, Hoke H, Idrissi A, Marekha BA, Moreau M, Honda Y, Umecky T, Shimomura T (2014) Microscopic interactions of the imidazolium-based ionic liquid with molecular liquids depending on their electron-donicity. Phys Chem Chem Phys 16:23627–23638
12. Marekha BA, Sonoda K, Uchida T, Tokuda T, Idrissi A, Takamuku T (2017) ATR-IR spectroscopic observation on intermolecular interactions in mixtures of imidazolium-based ionic liquids $C_n$mimTFSA ($n = 2$–12) with DMSO. J Mol Liq 232:431–439
13. Takamuku T, Tokuda T, Uchida T, Sonoda K, Marekha BA, Idrissi A, Takahashi O, Horikawa Y, Matsumura J, Tokushima T, Sakurai H, Kawano M, Sadakane K, Iwase H (2018) Hydrogen bonds of the imidazolium rings of ionic liquids with DMSO studied by NMR, soft X-ray spectroscopy, and SANS. Phys Chem Chem Phys 20:12858–12869
14. Shimomura T, Fujii K, Takamuku T (2010) Effects of the alkyl-chain length on the mixing state of imidazolium-based ionic liquid-methanol solutions. Phys Chem Chem Phys 12:12316–12324
15. Georg S, Billard I, Ouadi A, Gaillard C, Petitjean L, Picquet M, Solov'ev V (2010) Determination of successive complexation constants in an ionic liquid: complexation of $UO_2{}^{2+}$ with $NO_3{}^-$ in C_4mimTf_2N studied by UV-Vis spectroscopy. J Phys Chem B 114:4276–4282
16. Melchior A, Gaillard C, Gracia Lanas S, Tolazzi M, Billard I, Georg S, Sarrasin L, Boltoeva M (2016) Nickel(II) complexation with nitrate in dry [C_4mim][Tf_2N] ionic liquid: a spectroscopic, microcalorimetric, and molecular dynamics study. Inorg Chem 55:3498–3507
17. Kanzaki R, Uchida S, Kodamatani H, Tomiyasu T (2017) Copper(II) chloro complex formation thermodynamics and structure in ionic liquid, 1-butyl-3-methylimidazolium trifluoromethanesulfonate. J Phys Chem B 121:9659–9665
18. Kawazu Y, Hoke H, Yamada Y, Umecky T, Ozutsumi K, Takamuku T (2017) Complex formation of nickel(II) with dimethyl sulfoxide, methanol, and acetonitrile in a $TFSA^-$-based ionic liquid of [C_2mim][TFSA]. Phys Chem Chem Phys 19:31335–31344

19. Takamuku T, Sakurai H, Ogawa A, Tashiro A, Kawano M, Kawazu Y, Sadakane K, Iwase H, Ozutsumi K (2019) Effects of the long octyl chain on complex formation of nickel(II) with dimethyl sulfoxide, methanol, and acetonitrile in ionic liquid of [C_8mim][TFSA]. Phys Chem Chem Phys 21:3154–3163
20. Marquardt DW (1963) An algorithm for least-squares estimation of nonlinear parameters. J Soc Ind Appl Math 11:431–441
21. Suzuki H, Ishiguro S (1992) Thermodynamics and structures of nickel(II) chloro complexes in *N,N*-dimethylacetamide. Inorg Chem 31:4178–4183
22. Elaiwi A, Hitchcock PB, Seddon KR, Srinivasan N, Tan Y-M, Welton T, Zora JA (1995) Hydrogen bonding in imidazolium salts and its implications for ambient-temperature halogenoaluminate(III) ionic liquids. J Chem Soc Dalton Trans 21:3467–3472
23. Hardacre C, Holbrey JD, McMath SEJ, Bowron DT, Soper AK (2003) Structure of molten 1,3-dimethylimidazolium chloride using neutron diffraction. J Chem Phys 118:273–278
24. Fujii K, Kanzaki R, Takamuku T, Kameda Y, Kohara S, Kanakubo M, Shibayama M, Ishiguro S, Umebayashi Y (2011) Experimental evidences for molecular origin of low-Q peak in neutron/x-ray scattering of 1-alkyl-3-methylimidazolium bis(trifluoromethanesulfonyl)amide ionic liquids. J Chem Phys 135:244502
25. Triolo A, Russina O, Bleif HJ, Di Cola E (2007) Nanoscale segregation in room temperature ionic liquids. J Phys Chem B 111:4641–4644